Universiteit Leiden
The Netherlands

Ultrastructural characterization of maturing iPSC-derived nephron structures upon transplantation

Wiersma, L.E.; Avramut, M.C.; Koster, A.J.; Berg, C.W. van den; Rabelink, T.J.

RESEARCH ARTICLE

Ultrastructural characterization of maturing iPSC-derived nephron structures upon transplantation

L. E. Wiersma[1,2] | M. C. Avramut[1,3] | A. J. Koster[3] | C. W. van den Berg[1,2,4] | T. J. Rabelink[1,2,4]

[1]Department of Internal Medicine – Nephrology, Leiden University Medical Center, Leiden, The Netherlands

[2]Einthoven Laboratory of Vascular and Regenerative Medicine, Leiden University Medical Center, Leiden, The Netherlands

[3]Department of Cell and Chemical Biology - Electron Microscopy Facility, Leiden University Medical Center, Leiden, The Netherlands

[4]The Novo Nordisk Foundation Center for Stem Cell Medicine (reNEW), Leiden University Medical Center, Leiden, The Netherlands

Correspondence
C. W. van den Berg, Department of Internal Medicine – Nephrology, Leiden University Medical Center, Leiden, The Netherlands.
Email: c.w.van_den_berg@lumc.nl

Abstract

Pluripotent stem cell-derived kidney organoids hold great promise as a potential auxiliary transplant tissue for individuals with end-stage renal disease and as a platform for studying kidney diseases and drug discovery. To establish accurate models, it is crucial to thoroughly characterize the morphological features and maturation stages of the cellular components within these organoids. Nephrons, the functional units of the kidney, possess distinct morphological structures that directly correlate with their specific functions. High spatial resolution imaging emerges as a powerful technique for capturing ultrastructural details that may go unnoticed with other methods such as immunofluorescent imaging and scRNA sequencing. In our study, we have applied software capable of seamlessly stitching virtual slides generated from electron microscopy, resulting in high-definition overviews of tissue slides. With this technology, we can comprehensively characterize the development and maturation of kidney organoids when transplanted under the renal capsule of mice. These organoids exhibit advanced ultrastructural developments upon transplantation, including the formation of the filtration barrier in the renal corpuscle, the presence of microvilli in the proximal tubule, and various types of cell sub-segmentation in the connecting tubule similarly to those seen in the adult kidney. Such ultrastructural characterization provides invaluable insights into the structural development and functional morphology of nephron segments within kidney organoids and how to advance them by interventions such as a transplantation.

Research Highlights

- High-resolution imaging is crucial to determine morphological maturation of hiPSC-derived kidney organoids. Upon transplantation, refined ultrastructural development of nephron segments was observed, such as the development of the glomerular filtration barrier.

KEYWORDS
electron microscopy, iPSC-derived kidney organoids, regenerative medicine, transplantation, ultra-structural characterization

1 | INTRODUCTION

Nephrons of the kidney play a key role in homeostasis by regulating osmolarity and excretion of waste and toxins. These nephrons can be divided into different sections through which filtrate flows. The first section is the renal corpuscle, which is connected to the renal tubules. These tubules contain anatomically different segments, each with their own function, and are divided into the proximal tubule, loop of Henle, distal tubule, and the connecting tubule. Current treatment options for people suffering from end-stage renal disease are dialysis or receiving a kidney transplant. These treatments have major disadvantages as dialysis is very costly and time-consuming, and kidney transplantation is dependent on the availability of a compatible donor organ. The field of regenerative medicine aims to create auxiliary kidney tissues from pluripotent stem cells to provide a cell-based therapeutic approach.

Kidney organoids are a promising resource of transplantable functioning tissue (Kalejaiye et al., 2022). Upon transplantation in mice (Al-Awqati & Gao, 2011; Bantounas et al., 2018; Gupta et al., 2020) and chicken embryos or on chick chorioallantoic membrane (Garreta et al., 2019; Koning et al., 2022), the nephron structures of organoids further developed and matured. Upon transplantation, glomerular structures were able to exhibit size-selective sieving (van den Berg et al., 2020). This ability is heavily based on the correct structural development of the filtration barrier highlighting the importance of morphological maturation of the nephron.

Transplanted and untransplanted kidney organoids have previously been analyzed using, e.g., immunofluorescence imaging (Takasato et al., 2015; van den Berg et al., 2018), single-cell and bulk RNA sequencing (Combes et al., 2019; Koning et al., 2022; Subramanian et al., 2019; Wu et al., 2018), MALDI-MSI (Wang et al., 2022), and while these techniques are highly informative, they lack information on ultrastructural development and morphological specialization of specific cell types of each segment of the nephron. Here we performed ultrastructural high spatial resolution imaging using transmission electron microscopy (TEM) as a tool to describe morphological specialization in transplanted kidney organoids and provide an atlas focusing on the morphological development of the renal corpuscle and renal tubules.

2 | MATERIALS AND METHODS

2.1 | hiPSC culture and kidney organoid differentiation

Maintenance of hiPSCs and kidney organoid differentiation was performed as previously described (van den Berg et al., 2018). Briefly, hiPSC-CRL1502 clone C32 was cultured on vitronectin-coated plates in Essential 8 (E8) medium (Thermo Fisher Scientific). Cells were passaged twice a week with UltraPure EDTA (Thermo Fisher Scientific) for regular cell maintenance. For differentiation, cells were dissociated using TrypLE Select (Thermo Fisher Scientific) and plated at a density of 10,000 cells/cm^2 and cultured for 24 h in E8 medium with the addition of RevitaCell Supplement (Thermo Fisher Scientific).

Differentiation started with 8 μM CHIR99021 (R&D Systems) in STEMdiff APEL medium (APEL) (day 0). After 4 days, medium was switched to APEL medium containing 200 ng/mL rhFGF9 (R&D Systems) and 1 μg/mL heparin (Sigma-Aldrich). On day 7 of differentiation cells were incubated with 5 μM CHIR99021 in APEL medium for 1 h before dissociation with 0.25% Trypsin EDTA (Thermo Fisher Scientific). A total of 500,000 cells were pelleted and pipetted on a Transwell 0.4 μM pore polyester membrane (Corning). After 5 days, medium was switched to APEL medium without additives. In vitro organoid culture continued until transplantation on day 7 + 18.

2.2 | Animal experiments

All animal experiments were approved by the animal welfare committee of the Leiden University Medical Center. Immunodeficient nonobese diabetic/severe combined immunodeficiency mice (8 weeks old, Charles River Laboratories) were anesthetized with isoflurane, and the kidneys were temporarily exteriorized. A small incision was made in the renal capsule, and bisected kidney organoids of day 7 + 18 were placed under the kidney capsule. Temgesic (buprenorphine) was injected for pain relief. Samples were collected after 28 days of transplantation, unless stated otherwise.

2.3 | Adult human kidney

Two adult human kidneys (AHK) that were not accepted for transplantation and had research consent were used for tissue collection. AHK 1 had 11 min of warm storage followed by 20 h of static cold storage, and AHK 2 had 2 h of normothermic regional perfusion and 4 h of static cold storage before sampling. Briefly, normothermic regional perfusion is used during organ donation procedures and uses a cardiopulmonary bypass to restore flow of oxygenated blood, thereby circumventing warm ischemia. All images have been taken from AHK 2, unless otherwise indicated in the legend of the figure.

Kidneys were placed on ice for sampling and were dorsally sectioned with a surgical blade. 1×1 mm sections were taken from the cortex and medulla. All tissue samples were directly stored in fixatives for TEM.

2.4 | Transmission electron microscopy

Transplanted kidney organoids at day 28 after transplantation under mouse kidney capsule, and human kidney samples were fixed for 1.5 h at room temperature, with 1.5% glutaraldehyde (Electron Microscopy Sciences) in 0.1 M sodium-cacodylate buffered solution, pH 7.4. Subsequently, the tissues were rinsed 2× with 0.1 M sodium cacodylate-buffered solution and fixed for 1 h on ice with 1% osmium tetroxide (Electron Microscopy Sciences) in sodium cacodylate buffer.

—WILEY—

For some of the human kidney samples, an extra *en-bloc* staining step in 1% aqueous uranyl acetate was applied. Tissue samples were further washed 2× with demineralized water, twice with 70% ethanol, dehydrated overnight in 70% ethanol, then in 80% ethanol (10 min), 90% ethanol (10 min), and 100% ethanol absolute (twice 15 min; once 30 min). The probes were afterward infiltrated with 25%, 50%, 75% epon LX-112 (Ladd Research) in anhydrous acetone in steps of 30 min, followed by pure epon for 2 h, embedded in pure epon, mounted in BEEM capsules (Agar Scientific), and polymerized for 48 h at 60°C. Ultrathin sections (100 nm) were mounted onto copper slot grids, covered with formvar film and carbon layer, and then stained with an aqueous solution of 7% uranyl acetate for 20 min, followed by Reynold's lead citrate for 10 min. Samples were analyzed at an acceleration voltage of 120 kV using a Tecnai G^2 Spirit BioTWIN transmission electron microscope (FEI, now Thermo Fisher Scientific), equipped with a FEI 4 k Eagle CCD camera or on an FEI Tecnai G^2 12 TWIN electron microscope, equipped with a Gatan OneView camera (Gatan). Image mosaics of hundreds or even thousands of images each were recorded with binning 2 and stitched together using automated data acquisition and stitching software (Faas et al., 2012). These large-scale digital images give overviews of entire structures, providing also the possibility to zoom in to high detail for qualitative analysis. Virtual slides were analyzed using the Aperio ImageScope viewing software (Leica Biosystems).

3 | RESULTS

Day 7 + 18 organoids were bisected and transplanted under the renal capsule of mice. After 2–4 weeks, organoids were collected and fixed for transmission electron microscopy (TEM). Stitched images from TEM were analyzed and compared to literature and adult human kidney (AHK). Literature was based on human, rat, and rabbit kidney ultrastructure (Gilbert et al., 2017; Johnson et al., 2014; Mills, 2019; Ross & Pawlina, 2011; Verlander, 1998; Yu et al., 2020). Below we relay our findings on the ultrastructural development and maturation of each section of the nephron found in the transplanted kidney organoid (TKOR). To understand and compare our findings, we start each section with features found in AHK.

3.1 | Renal corpuscle

The renal corpuscle in the AHK comprises the glomerulus and Bowman's capsule (Figure S1A). The glomerulus contains capillary tufts and specialized epithelial cells (Figure S1B), while the Bowman's capsule encompasses a single parietal layer on the glomerulus' surrounding basement membrane (lamina basalis). The filtration barrier within the glomerular structure involves the glomerular endothelium, glomerular basement membrane (GBM), and glomerular epithelium (Figure S1C). The fenestrated glomerular endothelium allows the passage of various substances, including water, electrolytes, waste products, glucose, amino acids, and low-molecular-weight proteins, while retaining larger molecules.

The GBM consists of three layers: lamina rara interna, lamina densa, and lamina rara externa, oriented from capillary to visceral epithelial. Situated on the lamina rara externa are podocytes with foot processes that wrap around the capillary, forming filtration pores called filtration slits (Figure S1C). These filtration slits permit the passage of the glomerular filtrate while preventing larger molecules from crossing the barrier. The sub-podocyte space refers to the area beneath the podocyte, while the space between podocytes is known as the interpodocyte space. The peripheral urinary space denotes the space between the glomerular edge and the Bowman's capsule (Neal et al., 2005).

In TKOR, the glomerular structure is surrounded by a capsular epithelium indicating the Bowman's capsule and multiple capillaries can be observed in the glomerular structure (Figures 1a and S2). In the capillaries erythrocytes can be detected, confirming perfusion of blood through these capillaries. Closer observation of these capillaries shows the endothelium and their fenestration, which is crucial for the proper formation of the filtration barrier (Figure 1b and S2). Tri-lamination of the GBM with clearly defined dark and lighter layers marking the lamina rara interna, lamina densa, and lamina rara externa can also be observed. The GBM is smooth and appears to be very similar to the AHK counterpart (Figure S1B,C). Podocytes and foot processes with slit diaphragms of the TKOR sit on the GBM completely surrounding the capillary (Figures 1b and S2). They differ from these structures in the human kidney, as the foot processes are larger and not as numerous. In the TKOR, we were able to discern some interpodocyte space, but the sub-podocyte space and peripheral podocyte space cannot be observed as the overall glomerular structure is still compacted after 4 weeks of transplantation (Figures 1b and S2).

In summary, the renal corpuscle of the TKOR and the human kidney is very similar except for size and number of foot processes. The filtration barrier, fenestration of the glomerular endothelium, GBM, and specialization of the glomerular epithelium can be observed. A graphical overview of the filtration membrane in both TKOR and AHK can be found in Figure 1c.

3.2 | Proximal tubule

The proximal tubule in the AHK starts directly after the renal corpuscle and will predominantly reabsorb ultrafiltrate from the renal corpuscle. For this task, the tubule has a luminal brush border of long microvilli to increase the surface area of the cell (Figure S3). These long microvilli are highly characteristic of the proximal tubule and are not present in the other tubular segments. Other characteristics of the proximal epithelial are their elongated appearance with their nuclei situated at the basal side (Figure S3). Tight junctions at the apical side of the cells allow passive reabsorption of water and ions, and between the cells intercalated space can be observed. Just below the microvilli, vesicles, apical vacuoles, and lysosomes can be discriminated (Figure S3). These organelles are part of the endocytic/vacuolar-lysosomal system and largely responsible for the reabsorption and degradation of proteins that are taken up via endocytosis. In this
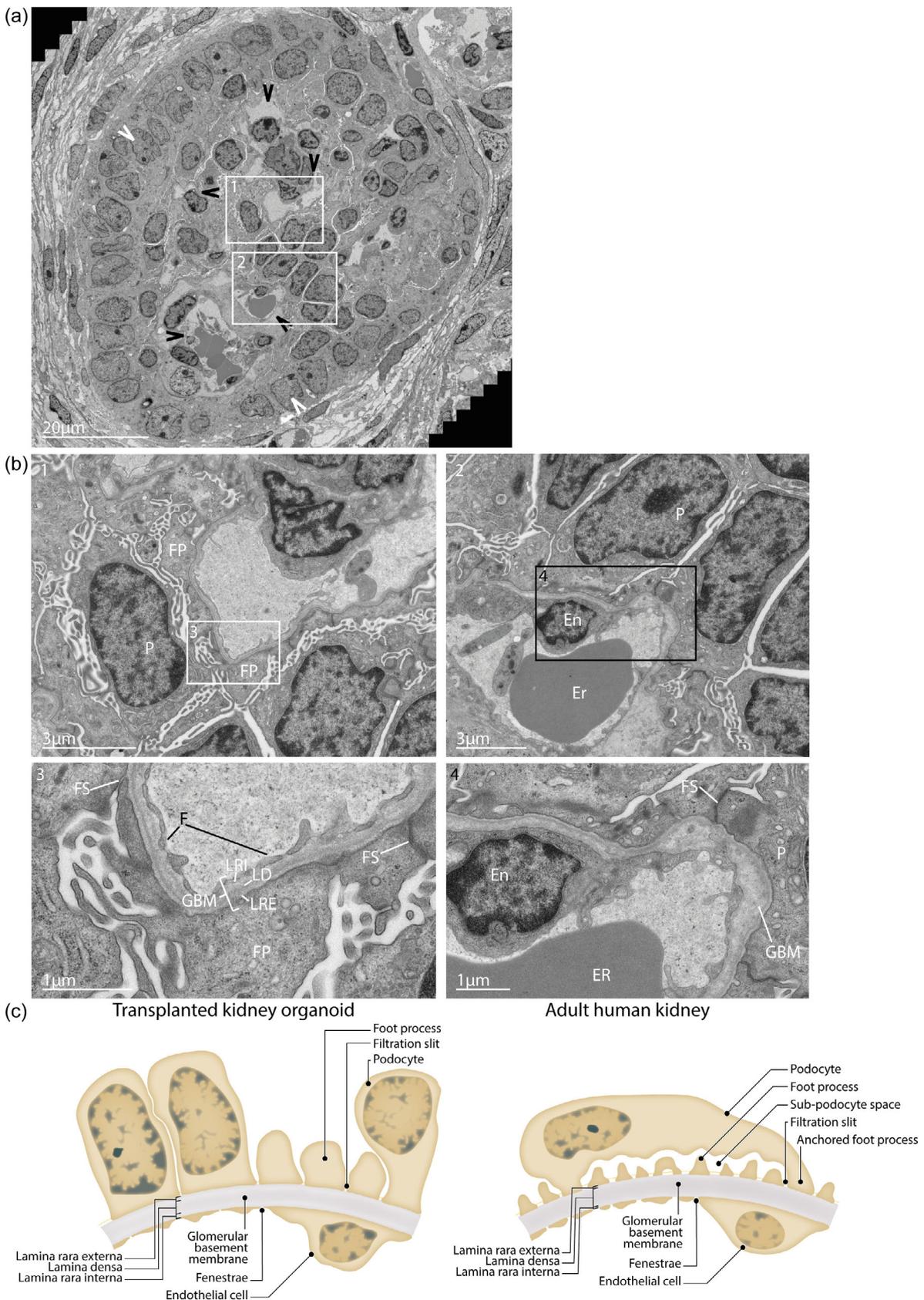
FIGURE 1 Development of the renal corpuscle of transplanted kidney organoids visualized using Transmission Electron Microscopy. (a) Overview image of a renal corpuscle in TKOR. Parietal cells (white arrowhead) line the glomerular structure indicating Bowman's capsule. Multiple glomerular capillaries are apparent (black arrowheads). (b) Magnified images (1 and 2) of the glomerular structure, in the TKOR. In the capillaries, endothelial cells (EN), fenestrae (F), and erythrocytes (ER) are observed. Podocytes (P), foot processes (FP), and filtration slits (FS) are seen on the glomerular basement membrane (GBM). Trilaminar GBM with lamina rara interna (LRI), lamina densa (LD), and lamina rara externa (LRE) are noted. (c) Graphical overview of the filtration barrier in the renal corpuscle in TKOR and AHK.

region, apical tubules which recycle receptors back to the membrane surface can also be found (not shown). The reabsorption and active transport require high amounts of energy, which is reflected by the large number of mitochondria in the cell and basolateral infoldings (Figure S3).

Proximal tubules in the TKOR after 4 weeks of transplantation show the characteristic elongated morphological shape, microvilli, tight junctions at the apical side, and nuclei primarily at the basal side of the cell (Figures 2a,b and S4). Vesicles can be seen just below the microvilli, as well as apical vacuoles and lysosomes that are part of the endocytic/vacuolar-lysosomal system, which shows the ability to degrade proteins. The TKOR exhibits a relatively lower number of mitochondria in the proximal tubule compared to the AHK. Basolaterally, junctions can be observed in individual cells of the TKOR (Figure 2c), but there are no infoldings or infoldings with mitochondria as observed in the AHK.

In the TKOR, we also observed, as expected, developing tubules that still exhibited a closed lumen (Figure S5A). We were not able to classify these tubules as they still lack most of the characteristic features of the tubular segments. For example, Figure S5A displays tubules with elongated cells that are close together, appear to be of the same type throughout the structure, and containing a few mitochondria. However, they do not express any microvilli, apical vacuoles, or other characteristic markers. In Figure S5B, we highlight presence of peritubular capillaries next to proximal tubular structures.

In Figure 2d, a graphical overview is provided, representing the most prominent features of proximal tubules in the TKOR and AHK.

3.3 | Loop of Henle and distal tubule

In the AHK, the loop of Henle is difficult to discriminate, and we were unable to find these tubules in our samples. According to literature (Gilbert et al., 2017; Johnson et al., 2014; Mills, 2019; Ross & Pawlina, 2011; Verlander, 1998; Yu et al., 2020), the loop of Henle consists of a thin descending and ascending limb that transitions to the thick ascending limb. The thin loop of Henle can be identified by the intense flattened and widened appearance of the cell and nuclei and the low number of cells in a cross section compared to the other tubules. The thin loop of Henle has tight junctions and is permeable to water. The thick loop of Henle is not permeable to water and consists of more elongated cells with more cuboidal, apically located nuclei. Both cells and nuclei are not as wide as the thin loop but can have a relatively wide appearance compared to the proximal or distal tubule. Cells in the thick loop of Henle also have many mitochondria, and basolateral infoldings with mitochondria as seen in the proximal tubule. The distal (convoluted) tubule is known as the diluting segment and finishes the filtrate. Based on literature (Gilbert et al., 2017; Johnson et al., 2014; Mills, 2019; Ross & Pawlina, 2011; Verlander, 1998; Yu et al., 2020), they have many similarities with the thick loop of Henle, making them difficult to distinguish from each other. The distal tubule has apical positioned nuclei and is filled with mitochondria, both in the cell body and the basolateral infoldings

(Figure S6). However, compared to the thick loop of Henle, the distal tubule cells are more elongated.

In TKOR, we found tubular structures that show characteristics representing developing thick loop of Henle or distal tubule (Figures 3a and S7). We characterized these tubules based on their lack of distinct morphological features such as microvilli or the presence of dark cells as seen in the connecting tubule. Other things to note were the low number of mitochondria, the lack of basolateral infoldings, some vesicles, and a junction at the basal membrane. We were unable to consistently observe more specific markers such as cuboidal nuclei and flattened or wide cells in our cross sections (Figures 3a and S7) and could not further distinguish these structures in the TKOR. We were able to find one tubule with characteristics of the thick loop of Henle in the TKOR based on the widened appearance of some of the cells and nuclei after 14 days of transplantation (Figure S8). Furthermore, due to the wide shape of the cells, there were fewer cells observed in a cross section when compared to the proximal tubule or distal tubule. The graphical representation in Figure 3b shows developing thick loop of Henle or distal tubule in the TKOR and the thick loop of Henle and distal tubule in AHK.

3.4 | Connecting tubule and collecting duct system

In the AHK, the connecting tubule is the transitional segment which joins the distal tubule and the collecting duct. We were unable to distinguish the connecting tubule and collecting duct based on TEM imaging. Both the connecting tubule and the collecting duct have intercalated cells. Intercalated cells are characterized by their dark cytoplasm and nuclei in AHK (Figure S9). Intercalated cells can be subdivided into α-intercalated cells (which secrete acid (H^+)) and β-intercalated cells (which secrete bicarbonate (HCO_3)). The α-intercalated cells have notable villi on the apical membrane and tubulovesicular structures just beneath the apical surface, while the β-intercalated cells lack these tubulovesicular structures and have a more smooth apical membrane. Both have a high number of mitochondria and basolateral infoldings without mitochondria, and lysosomes can be present (based on literature (Gilbert et al., 2017; Johnson et al., 2014; Mills, 2019; Ross & Pawlina, 2011; Verlander, 1998; Yu et al., 2020)). In our images, we were unable to make a clear distinction between the α- and β-intercalated cells. Next to intercalated cells, the connecting tubule has connecting tubule cells, and the collecting duct has principal cells. Connecting tubule cells are specific to the connecting tubule, and have a few short microvilli, contain a few mitochondria and lysosomes. These cells have the same characteristics as the principal cells of the collecting duct, but the latter cells have basolateral infoldings that are lacking in connecting tubule cells (based on literature (Gilbert et al., 2017; Johnson et al., 2014; Mills, 2019; Ross & Pawlina, 2011; Verlander, 1998; Yu et al., 2020)).

In the kidney organoid, we are able to observe connecting tubule, but not the collecting duct, which has been demonstrated by single cell RNA sequencing analysis in transplanted and untransplanted
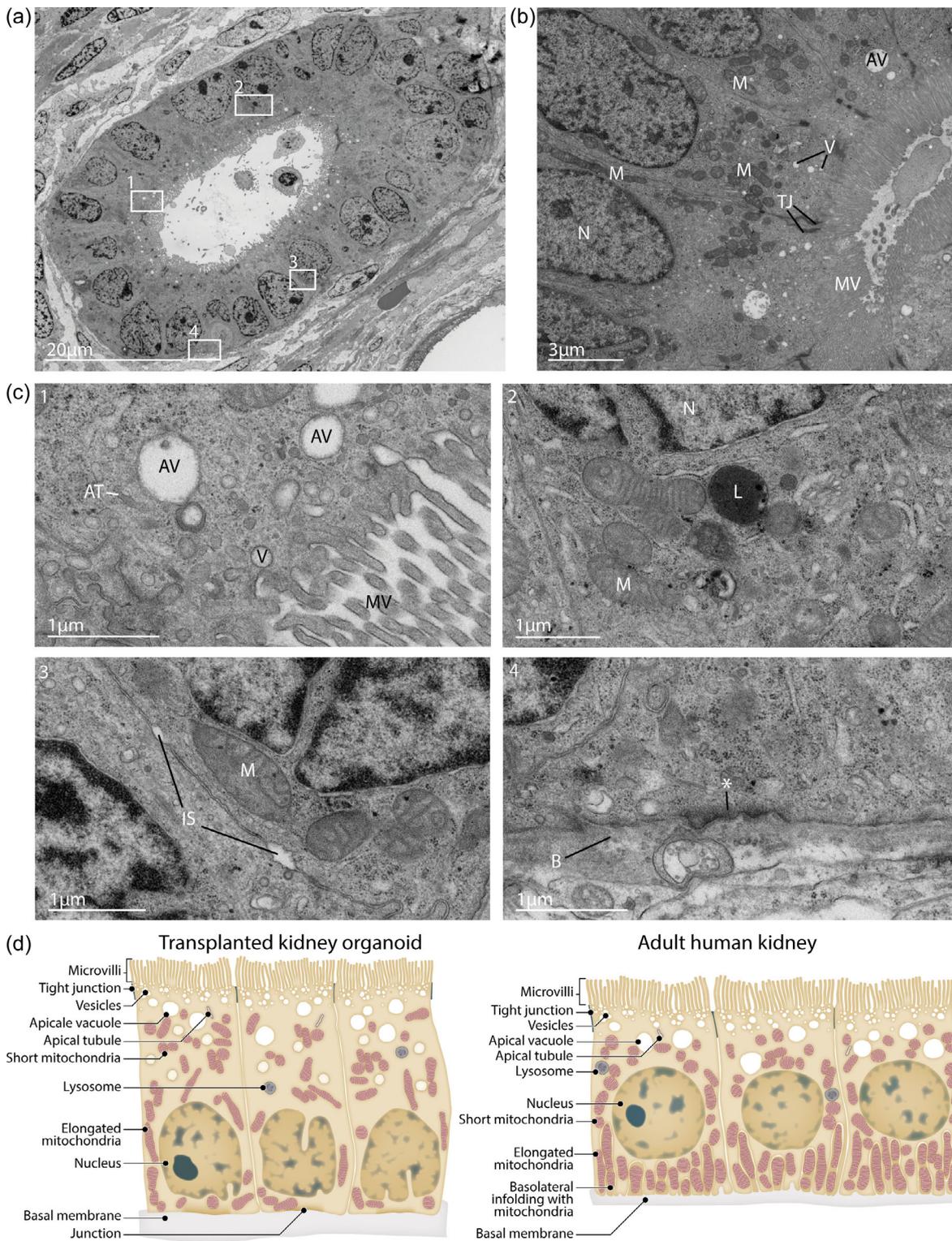
FIGURE 2 Well developed proximal tubule in transplanted kidney organoids visualized using Transmission Electron Microscopy. (a) Overview image of proximal tubule in TKOR showing an aligned epithelial layer consisting of 1 type of cells with microvilli and apical vacuoles at the luminal side and nuclei at the basolateral side. (b) Magnified image of proximal tubular epithelial cell in TKOR. At the luminal side, the microvilli (MV), vesicles (V), apical vacuoles (AV) and tight junctions (T) are visible. The cell contains few mitochondria (M). (C) Multiple images of cellular structures of the proximal in TKOR (From A). At this level the apical tubules (AT), apical vacuoles (AV), vesicles (V), lysosomes (L) of the endocytic/vacuolar-lysosomal system are visible under the microvilli (MV), and mitochondria (M) and intercalated space (IS) can also be observed. At the basal membrane (B) a junction can be noted (*). (d) Graphical overview illustrating the similarities and differences between the proximal tubular cells in TKOR and the human kidney.
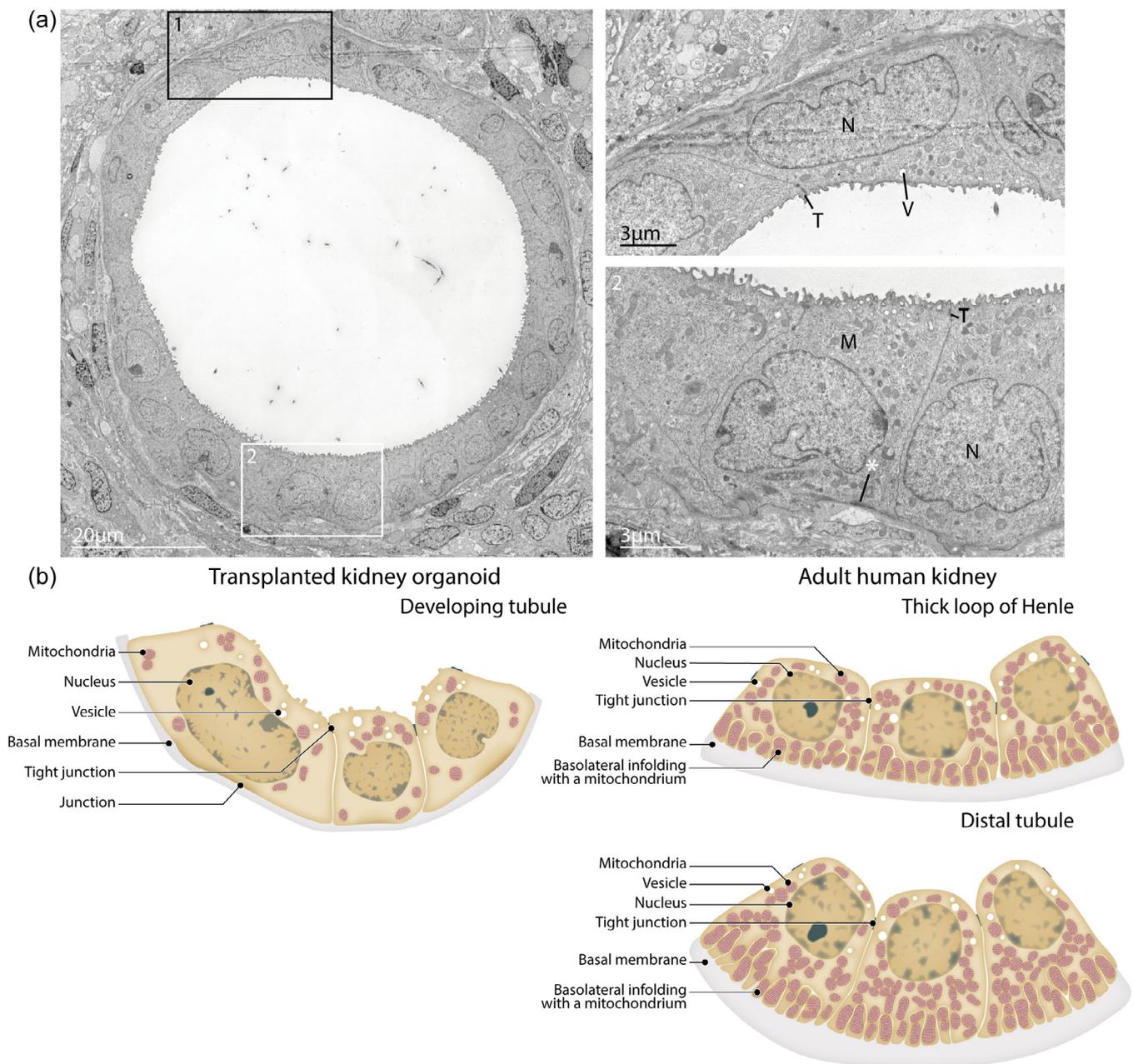
FIGURE 3 Developing Loop of Henle or distal tubule in transplanted kidney organoids visualized with Transmission Electron Microscopy. (a) Overview image of tubular structures in TKOR considered as developing loop of Henle or distal tubule. Tight junctions (T) are at the top of the cell, and at the basal membrane a junction can be observed (*). Mitochondria (M) and vesicles (V) can be observed in the cytoplasm. (b) Graphical overview of the developing loop of Henle/distal tubule in TKOR and the thick loop of Henle and distal tubule in AHK.

kidney organoids in previous studies (Koning et al., 2022; Subramanian et al., 2019; Wu et al., 2018). Interestingly, in TKOR, we were able to observe connecting tubules in high abundance (Figures 4a and S10). These tubules could be readily identified by the difference in color of the cells in cross sections, where intercalated cells had a dark cytoplasm and nuclei (Figure 4b) and the connecting tubule cells were much lighter (Figure 4c). Strikingly, in the TKOR, we observed two types of intercalated cells based on their morphology (Figure 4b). Variant 1 has a more flattened appearance, where variant 2 is more rounded. Overall, the endoplasmic reticulum in these cells is

dilated, but more severely in variant 1 than variant 2. It is unclear whether these intercalated cells are two different types as seen in the AHK or are representations of different developmental stages of these cells. Interestingly, several intercalated cells have a high number of mitochondria (Figures 4d and S10). This is in contrast with the other cells of the TKOR, where a relatively low number of mitochondria was observed, especially compared to the AHK.

The connecting tubule cells have a light color, their endoplasmic reticulum is not dilated like the intercalated cells, contain vesicles, and have a junction at the basal membrane (Figures 4c and S10). Overall,
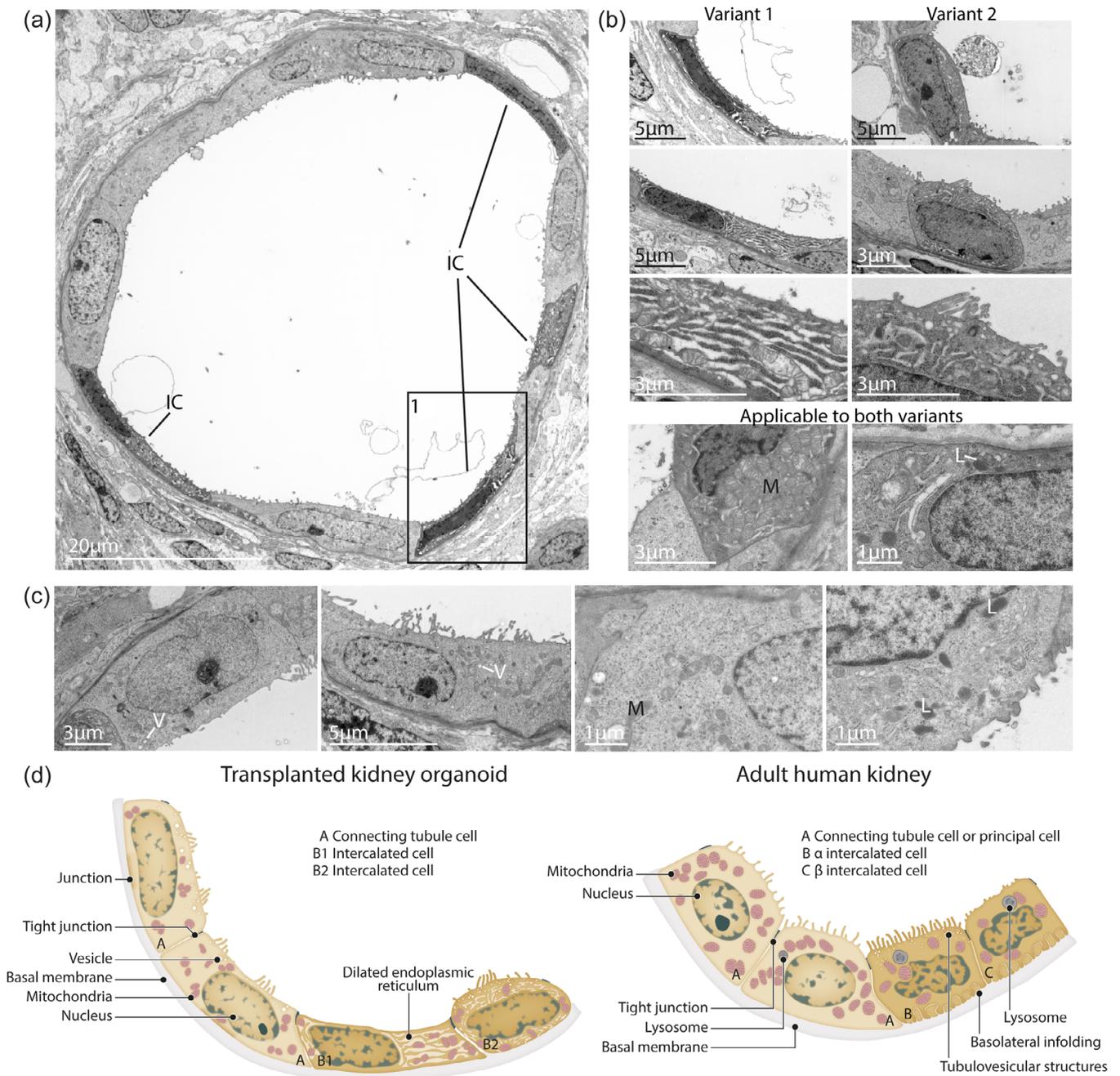
FIGURE 4 Connecting tubule in transplanted kidney organoids visualized using Transmission Electron Microscopy. (A) Overview image of a connecting tubule in TKOR showing an aligned epithelial layer consisting of intercalated cells (IC) and connecting tubule cells that can be distinguished by the brightness of the cell. The darker cells are the intercalated cells, and the lighter cells are the connecting tubule cells. (b) Magnified images focusing on intercalated cells in TKOR. Intercalated cells have a dark appearance in both cytoplasm and nuclei. Two variants were observed; variant one has a darker and more flattened appearance than variant 2 with a rounded appearance. In both variants, the endoplasmic reticulum is dilated. Both variants have mitochondria (M) with some lysosomes (L), a nucleus (N), and tight junctions at the top of the cells. (c) Magnified images focusing on connecting tubule cell in TKOR. Connecting tubule cells are lighter in color in both cytoplasm and nuclei compared to the intercalated cell, containing a few organelles like mitochondria (M), lysosomes (L), vesicles (V), and a nucleus(N), junction at the basal membrane (*), and tight junctions (T). (d) Graphical overview illustrating the similarities and differences between the connecting tubule of TKOR and human kidney.

the cells have fewer organelles with just a few mitochondria and lysosomes, which is comparable to these structures in the AHK. In Figure 4e, a graphical overview with the distinctive markers of the connecting tubule markers of the AHK and TKOR is displayed.

4 | DISCUSSION

High spatial resolution imaging has played a crucial role in the ultrastructural characterization of transplanted kidney organoids. This

technique allows us to observe and analyze the morphological development of nephron segments at a cellular level, providing valuable insights into their functional morphology, such as the development of the glomerular filtration barrier, microvilli on the proximal tubule, and cell type specification in connecting tubule. While the transcription profiles of iPSC-derived kidney organoids resemble those of early-stage kidneys, their complete maturation requires a natural environment with proper environmental cues and stimuli.

In embryonic development, the nephron is completed in the third trimester after 32 to 36 weeks (Hinchliffe et al., 1991). iPSC-derived kidney organoids in vitro have transcription profiles resembling the kidney in the first trimester (Takasato et al., 2015). Importantly, environmental ques, structurally, flow, supply of nutrients, or others, play essential roles in the proper further development of stem cell-derived tissues. Upon transplantation in either mice (organoid age day 7 + 18 (Gupta et al., 2020; van den Berg et al., 2018), or d7 + 12/19 (Bantounas et al., 2018)), in celomic cavity of chicken embryos (day 7 + 12 (Koning et al., 2022)) or on the CAM (age day 16 (Garreta et al., 2019)), kidney organoids show a great degree of maturation. While maturation of TKOR nephron structures can be assessed based on expression of markers for maturation, morphological development on a cellular level is even more important. We therefore compared nephron structures of the TKOR to AHK with high spatial resolution images, allowing for ultrastructural characterization. We opted to use fetal kidney as reference material. However, more literature is available on electron microscopy of adult kidney tissue, and the level of maturation in fetal tissue is highly dependent on the age and stage of nephrogenesis of the available fetal tissue when using it as reference material. While complete maturation of TKOR to an adult-like stage of nephron structures cannot be expected upon transplantation for 4 weeks, we previously described advanced maturation of the renal corpuscle, proximal and connecting tubules (van den Berg et al., 2018). Vascularization of the glomerular structures resulted in the formation of the filtration barrier with the fenestrated endothelium, tri-laminar GBM, and podocytes with foot processes. We functionally characterized these tissues and showed that the glomeruli matured to such an extent that these are able to perform size selective sieving (van den Berg et al., 2020).

The morphological characteristics of each tubular segment, including gene and protein expression, are distinct and essential for their respective functions. In the proximal tubule of the TKOR, we observed well-developed microvilli and a prominent lysosomal/endocytic system, indicating proper development. A further distinction in S1, S2 and S3 segments could, however, not be made on basis of the TEM pictures in these developing and maturing kidney organoids.

In the TKOR, we were able to identify the presence of developing loops of Henle and distal tubules. Even in the AHK, to distinguish these tubules can be challenging, and in our organoid tissue, we faced difficulties in clearly differentiating between them. The connecting tubule exhibited distinct characteristics, such as specialized intercalated cells. In the TKOR, variations in intercalated cell types were observed, but we currently cannot definitively identify them as α- or β-intercalated cells. The connecting tubule plays a crucial role in connecting the nephron to the collecting duct. Establishing a well-defined connecting segment could be particularly relevant for future transplantation experiments. During development, the connecting tubule bridges the newly developed nephrons to the collecting duct system, which originates from a separate progenitor population known as the ureteric bud, distinct from the mesodermal origin of the rest of the nephron.

After a mere 4 weeks of transplantation, we previously observed that the nephron structures in the TKOR have undergone significant development compared to untransplanted tissues (van den Berg et al., 2018), yet they are still in a phase of maturation. While several crucial characteristics can be observed, some features are still absent. For instance, even though all cells contained mitochondria, they were not as abundant as in the AHK. However, the most notable difference we observed was the absence of any form of basolateral infolding, with or without mitochondria. We did find junctions at the basal membrane of most cells. We hypothesize that altering the protocol or adjusting the media to align with the metabolic needs of kidney cells (Vanslambrouck et al., 2022; Wang et al., 2022), the age of the organoid at time of transplantation, or extending the time of transplantation could help the development of more mature nephron structures.

Our paper describes the ultrastructural development of transplanted kidney organoids, and this morphology-based atlas could be used as a source for future artificial intelligence-based approaches (Holscher et al., 2023). Technological advances in the automation of morphology annotation could pave the way for the availability of automated quantitative analysis of morphologies for ultrastructural characterization of iPSC-derived nephron structures. A prerequisite for these methodological developments is the availability of large-scale, high-resolution image data obtained under well-defined conditions. The provided image data atlases, together with the accompanying characterization of the morphologies described, provide a rich source for these technological developments.

In summary, high spatial resolution imaging allows us to analyze the structural development and functional morphology of nephron segments in transplanted kidney organoids. These tissues exhibit more mature nephron structures, which hold promise for their potential therapeutic use in patients. Understanding the ultrastructural characteristics of these organoids is vital for ensuring their functionality and effectiveness in clinical applications.

AUTHOR CONTRIBUTIONS

L. E. Wiersma: Writing – original draft; methodology; conceptualization; visualization; validation. **M. C. Avramut:** Methodology; validation; investigation. **A. J. Koster:** methodology, writing – review and editing. **C. W. van den Berg:** Conceptualization; investigation; supervision; writing – review and editing; validation; methodology. **T. J. Rabelink:** Supervision; writing – review and editing; funding acquisition; methodology.

ACKNOWLEDGMENTS

CONFLICT OF INTEREST STATEMENT

Al authors have no conflict of interest to disclose.

DATA AVAILABILITY STATEMENT

The data that support the findings of this study are available from the corresponding author upon reasonable request.

ORCID

L. E. Wiersma https://orcid.org/0000-0002-4197-9759
C. W. van den Berg https://orcid.org/0000-0002-4419-3428

REFERENCES

Al-Awqati, Q., & Gao, X. B. (2011). Differentiation of intercalated cells in the kidney. *Physiology (Bethesda)*, 26(4), 266–272. https://doi.org/10.1152/physiol.00008.2011

Bantounas, I., Ranjzad, P., Tengku, F., Silajdzic, E., Forster, D., Asselin, M. C., Lewis, P., Lennon, R., Plagge, A., Wang, Q., Woolf, A. S., & Kimber, S. J. (2018). Generation of functioning nephrons by implanting human pluripotent stem cell-derived kidney progenitors. *Stem Cell Reports*, 10(3), 766–779. https://doi.org/10.1016/j.stemcr.2018.01.008

Combes, A. N., Zappia, L., Er, P. X., Oshlack, A., & Little, M. H. (2019). Single-cell analysis reveals congruence between kidney organoids and human fetal kidney. *Genome Med*, 11(1), 3. https://doi.org/10.1186/s13073-019-0615-0

Faas, F. G., Avramut, M. C., van den Berg, B. M., Mommaas, A. M., Koster, A. J., & Ravelli, R. B. (2012). Virtual nanoscopy: Generation of ultra-large high resolution electron microscopy maps. *Journal of Cell Biology*, 198(3), 457–469. https://doi.org/10.1083/jcb.201201140

Garreta, E., Prado, P., Tarantino, C., Oria, R., Fanlo, L., Marti, E., Zalvidea, D., Trepat, X., Roca-Cusachs, P., Gavalda-Navarro, A., Cozzuto, L., Campistol, J. M., Izpisua Belmonte, J. C., Hurtado Del Pozo, C., & Montserrat, N. (2019). Fine tuning the extracellular environment accelerates the derivation of kidney organoids from human pluripotent stem cells. *Nature Materials*, 18(4), 397–405. https://doi.org/10.1038/s41563-019-0287-6

Gilbert, S. F., Weiner, D. E., Bomback, A. S., Perazella, M. A., & Tonelli, M. (2017). *National kidney foundation primer on kidney diseases* (7th ed.). Elsevier.

Gupta, A. K., Sarkar, P., Wertheim, J. A., Pan, X. C., Carroll, T. J., & Oxburgh, L. (2020). Asynchronous mixing of kidney progenitor cells potentiates nephrogenesis in organoids. *Communications Biology*, 3(1), 231. https://doi.org/10.1038/s42003-020-0948-7

Hinchliffe, S. A., Sargent, P. H., Howard, C. V., Chan, Y. F., & van Velzen, D. (1991). Human intrauterine renal growth expressed in absolute number of glomeruli assessed by the disector method and Cavalieri principle. *Laboratory Investigation*, 64(6), 777–784. https://www.ncbi.nlm.nih.gov/pubmed/2046329

Holscher, D. L., Bouteldja, N., Joodaki, M., Russo, M. L., Lan, Y. C., Sadr, A. V., Cheng, M., Tesar, V., Stillfried, S. V., Klinkhammer, B. M., Barratt, J., Floege, J., Roberts, I. S. D., Coppo, R., Costa, I. G., Bulow, R. D., & Boor, P. (2023). Next-generation morphometry for pathomics-data mining in histopathology. *Nature Communications*, 14(1), 470. https://doi.org/10.1038/s41467-023-36173-0

Johnson, R. J., Feehally, J., & Floege, J. (2014). *Comprehensive clinical nephrology* (5th ed.). Saunders.

Kalejaiye, T. D., Barreto, A. D., & Musah, S. (2022). Translating organoids into artificial kidneys. *Current Transplantation Reports*, 9(4), 276–286. https://doi.org/10.1007/s40472-022-00383-0

Koning, M., Dumas, S. J., Avramut, M. C., Koning, R. I., Meta, E., Lievers, E., Wiersma, L. E., Borri, M., Liang, X., Xie, L., Liu, P., Chen, F., Lin, L., Luo, Y., Mulder, J., Spijker, H. S., Jaffredo, T., van den Berg, B. M., Carmeliet, P., ... Rabelink, T. J. (2022). Vasculogenesis in kidney organoids upon transplantation. *NPJ Regenerative Medicine*, 7(1), 40. https://doi.org/10.1038/s41536-022-00237-4

Mills, E. S. (2019). *Histology for pathologists* (5th ed.). Lippincott Williams & Wilkins.

Neal, C. R., Crook, H., Bell, E., Harper, S. J., & Bates, D. O. (2005). Three-dimensional reconstruction of glomeruli by electron microscopy reveals a distinct restrictive urinary subpodocyte space. *Journal of the American Society of Nephrology*, 16(5), 1223–1235. https://doi.org/10.1681/ASN.2004100822

Ross, M. H., & Pawlina, W. (2011). *Histology: A text and atlas; with correlated cell and molecular biology* (6th ed.). Wolters Kluwer/Lippincott Williams & Wilkins.

Subramanian, A., Sidhom, E. H., Emani, M., Vernon, K., Sahakian, N., Zhou, Y., Kost-Alimova, M., Slyper, M., Waldman, J., Dionne, D., Nguyen, L. T., Weins, A., Marshall, J. L., Rosenblatt-Rosen, O., Regev, A., & Greka, A. (2019). Single cell census of human kidney organoids shows reproducibility and diminished off-target cells after transplantation. *Nature Communications*, 10(1), 5462. https://doi.org/10.1038/s41467-019-13382-0

Takasato, M., Er, P. X., Chiu, H. S., Maier, B., Baillie, G. J., Ferguson, C., Parton, R. G., Wolvetang, E. J., Roost, M. S., de Sousa, C., Lopes, S. M., & Little, M. H. (2015). Kidney organoids from human iPS cells contain multiple lineages and model human nephrogenesis. *Nature*, 526(7574), 564–568. https://doi.org/10.1038/nature15695

van den Berg, C. W., Koudijs, A., Ritsma, L., & Rabelink, T. J. (2020). In vivo assessment of size-selective glomerular sieving in transplanted human induced pluripotent stem cell-derived kidney organoids. *Journal of the American Society of Nephrology*, 31(5), 921–929. https://doi.org/10.1681/ASN.2019060573

van den Berg, C. W., Ritsma, L., Avramut, M. C., Wiersma, L. E., van den Berg, B. M., Leuning, D. G., Lievers, E., Koning, M., Vanslambrouck, J. M., Koster, A. J., Howden, S. E., Takasato, M., Little, M. H., & Rabelink, T. J. (2018). Renal subcapsular transplantation of PSC-derived kidney organoids induces neo-vasculogenesis and significant glomerular and tubular maturation in vivo. *Stem Cell Reports*, 10, 751–765. https://doi.org/10.1016/j.stemcr.2018.01.041

Vanslambrouck, J. M., Wilson, S. B., Tan, K. S., Groenewegen, E., Rudraraju, R., Neil, J., Lawlor, K. T., Mah, S., Scurr, M., Howden, S. E., Subbarao, K., & Little, M. H. (2022). Enhanced metanephric specification to functional proximal tubule enables toxicity screening and infectious disease modelling in kidney organoids. *Nature Communications*, 13(1), 5943. https://doi.org/10.1038/s41467-022-33623-z

Verlander, J. W. (1998). Normal ultrastructure of the kidney and lower urinary tract. *Toxicologic Pathology*, 26(1), 1–17. https://doi.org/10.1177/019262339802600101

Wang, G., Heijs, B., Kostidis, S., Rietjens, R. G. J., Koning, M., Yuan, L., Tiemeier, G. L., Mahfouz, A., Dumas, S. J., Giera, M., Kers, J., de Sousa, C., Lopes, S. M., van den Berg, C. W., van den Berg, B. M., & Rabelink, T. J. (2022). Spatial dynamic metabolomics identifies metabolic cell fate trajectories in human kidney differentiation. *Cell Stem Cell*, *29*(11), 1580–1593. https://doi.org/10.1016/j.stem.2022.10.008

Wu, H., Uchimura, K., Donnelly, E. L., Kirita, Y., Morris, S. A., & Humphreys, B. D. (2018). Comparative analysis and refinement of human PSC-derived kidney organoid differentiation with single-cell transcriptomics. *Cell Stem Cell*, *23*(6), 869–881 e868. https://doi.org/10.1016/j.stem.2018.10.010

Yu, A. S. L., Chertow, G. M., Luyckx, V. A., Marsden, P. A., Skorecki, K., & Taal, M. W. (2020). *Brenner & Rector's the kidney* (7th ed.). Elsevier.

SUPPORTING INFORMATION

Additional supporting information can be found online in the Supporting Information section at the end of this article.